

# Chemical Science

Volume 16  
Number 26  
14 July 2025  
Pages 11683–12198

[rsc.li/chemical-science](https://rsc.li/chemical-science)



ISSN 2041-6539




**EDGE ARTICLE**

Erwin Reisner *et al.*  
Adapting gas fermenting bacteria for light-driven domino  
valorization of CO<sub>2</sub>

Cite this: *Chem. Sci.*, 2025, 16, 11801

All publication charges for this article have been paid for by the Royal Society of Chemistry

## Adapting gas fermenting bacteria for light-driven domino valorization of CO<sub>2</sub>†

Lin Su,  ‡§ Santiago Rodríguez-Jiménez,  § Marion I. M. Short and Erwin Reisner  \*

The solar-driven valorization of CO<sub>2</sub> to fuels and chemicals provides an exciting opportunity to develop a circular chemical industry, but the controlled production of multicarbon organics remains a major challenge. Here, we present an abiotic–biotic domino strategy that integrates a photocatalytic CO<sub>2</sub>-to-syngas conversion system with evolved syngas-fermenting bacteria to enable the upcycling of CO<sub>2</sub> into valuable C<sub>2</sub> products, including acetate and ethanol. To optimize microbial syngas fermentation through an accessible and chemist-friendly platform, we employ adaptive laboratory evolution (ALE) of *Clostridium ljungdahlii* (Cl). The adapted strain, Cl<sub>adapt</sub>, exhibits a 2.5-fold increase in growth rate and a 120-fold enhancement in C<sub>2</sub> production compared to the wild type (Cl<sub>wt</sub>). Isotopic labeling confirmed Cl<sub>adapt</sub>'s high conversion efficiency, yielding 6:1 and 9:1 ratios of <sup>13</sup>C: <sup>12</sup>C in acetate and ethanol, respectively. Whole genome sequencing revealed mutations in Cl<sub>adapt</sub>, offering initial clues to its enhanced metabolism. A scaled-up semiconductor–molecule hybrid photocatalyst, TiO<sub>2</sub>|phosphonated Co(terpyridine)<sub>2</sub>, was employed to generate sufficient syngas (CO/H<sub>2</sub> ratio: ~30:70 with 1.3 mmol of CO after 6 days) for Cl<sub>adapt</sub> to demonstrate photocatalytic CO<sub>2</sub> → syngas → C<sub>2</sub> conversion (yielding 0.46 ± 0.07 mM, or 3.2 μmol, of acetate). This study offers a streamlined approach to improving syngas fermentation in Cl, insights into microbial adaptability, and an ALE-guided pathway for solar-powered CO<sub>2</sub> upcycling using an inorganic–microbial domino strategy.

Received 28th January 2025  
Accepted 10th May 2025

DOI: 10.1039/d5sc00764j

rsc.li/chemical-science

## Introduction

Semi-biological photosynthesis merges synthetic and microbial approaches to produce sustainable fuels using sunlight, particularly excelling in selective multicarbon product formation *via* the metabolic pathways available through biocatalysis.<sup>1,2</sup> Several recent reports demonstrate the promise and feasibility of this emerging approach: A hybrid solar water splitting–biosynthetic system uses green H<sub>2</sub> as intermediate to fix CO<sub>2</sub> and efficiently produce biomass and fuels using *Cupriavidus necator*.<sup>3</sup> Coupling a synthetic photocatalyst with *Shewanella oneidensis* resulted in selective hydrogenation of C=C and C=O bonds.<sup>4</sup> The photosensitization of *Moorella thermoacetica* with extracellular CdS or intracellular gold nanoclusters established a pathway for bacterial CO<sub>2</sub> utilization, integrating microbial systems with nanomaterials to enhance photosynthetic efficiency.<sup>5,6</sup>

Gas fermenting acetogenic bacteria, particularly *Clostridium* species, have emerged as versatile platforms to produce biofuels and biochemicals from syngas, a mixture of H<sub>2</sub>, CO and CO<sub>2</sub>.<sup>7–9</sup> These *Clostridium* strains utilize the Wood–Ljungdahl pathway, which consists of two branches to produce the C<sub>2</sub> compounds (Fig. 1A): the methyl branch, reducing CO<sub>2</sub> to formate and further to a methyl group, and the carbonyl branch, which forms an acetyl group from CO. *Clostridium ljungdahlii* (Cl) has shown promise in fermenting these gases into valuable products, underscoring the economic viability of this approach in biotechnology. For instance, a carbon-negative fermentation process was established using engineered and closely related *Clostridium autoethanogenum* to convert waste gas feedstocks into acetone and isopropanol with high efficiency.<sup>10</sup> An Ag-catalyst based gas diffusion electrolyzer for CO<sub>2</sub>-to-syngas conversion was coupled with syngas-fermenting *C. autoethanogenum* and *C. kluyveri*, producing butanol and hexanol with high selectivity and therefore offers a sustainable pathway for industrial chemical production from CO<sub>2</sub> and water using renewable energy.<sup>11</sup>

To further harness and optimize the metabolic capabilities of these microorganisms, adaptive laboratory evolution (ALE) emerges as a powerful tool to select and enhance beneficial traits without the need for genetic engineering. The principles and applications of ALE have demonstrated its simplicity and efficacy in tailoring microbial phenotypes for improved

Yusuf Hamied Department of Chemistry, University of Cambridge, Cambridge, UK.  
E-mail: reisner@ch.cam.ac.uk

† Electronic supplementary information (ESI) available. See DOI: <https://doi.org/10.1039/d5sc00764j>

‡ Present address: School of Biological and Behavioural Sciences, Queen Mary University of London, Mile End Road, London E1 4NS, UK.

§ These authors contributed equally to this work.

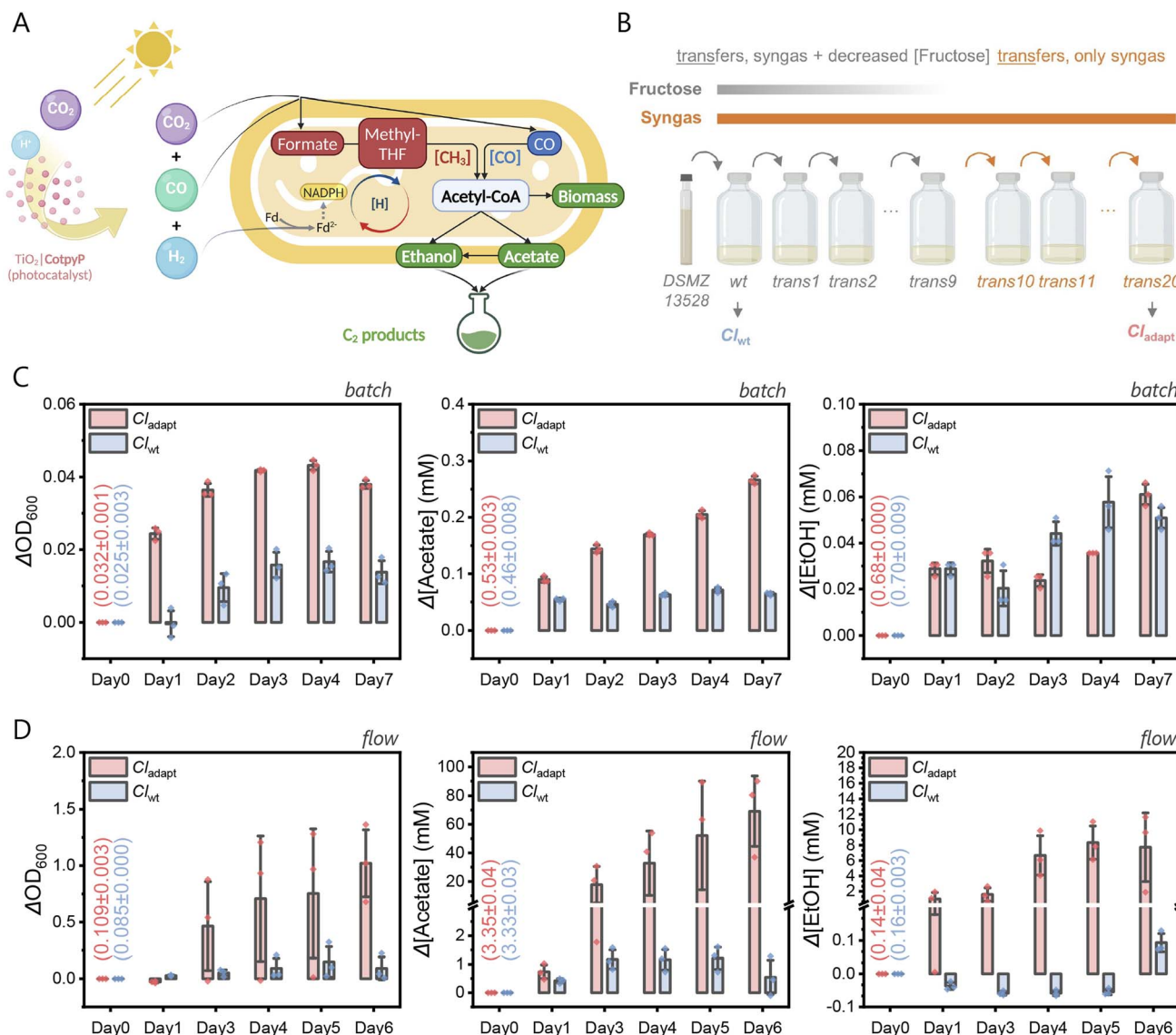


Fig. 1 Adaptive laboratory evolution (ALE) of *C. ljungdahliae*. (A) Schematic illustration of the syngas-fermenting metabolic pathways in *C. ljungdahliae* (*Cl*), including integration with photocatalytic syngas production.  $[\text{CH}_3]$  (red color), methyl branch;  $[\text{CO}]$  (blue color), carbonyl branch. (B) Schematic summary of the ALE process. The wild-type strain ( $Cl_{wt}$ ) was adapted to a syngas environment through gradual fructose reduction and removal over 20 transfers, resulting in the adapted strain ( $Cl_{adapt}$ ). (C) Comparative analysis of growth and  $\text{C}_2$  product generation (acetate and ethanol) between  $Cl_{adapt}$  and  $Cl_{wt}$  under batch gas purging conditions (syngas purging for 30 min daily, 112 mL headspace). (D) Similar comparative analysis under continuous gas flow conditions (10 mL syngas per min). Growth conditions: ATCC Medium 1754 (pH 5.9), 37 °C with 150 rpm mixing. Numbers in brackets indicate the values at the start of the experiment.

industrial performance.<sup>12,13</sup> Examples of successful ALE applications illustrate the transferability, flexibility and transformative potential of ALE in metabolic engineering and synthetic biology.<sup>14–19</sup> For example, ALE of *Sporomusa ovata* integrated with light-harvesting silicon nanowires led to a 2.4-fold increase in  $\text{CO}_2$ -reducing current density, enhancing bio-electrochemical  $\text{CO}_2$  reduction.<sup>16</sup> Similarly, *C. autoethanogenum* strains developed through ALE showed superior growth and product profiles in continuous bioreactor cultures.<sup>19</sup> ALE using  $\text{CO}_2$  and  $\text{H}_2$ , with other *C. autoethanogenum* lineages exposed to 2%  $\text{CO}$ , has also significantly enhanced growth rates and ethanol production, revealing extensive proteome and

metabolome changes that highlight new targets for metabolic engineering.<sup>20</sup>

Here, we explore the synergistic potential of ALE-derived gas-fermenting bacteria and photocatalysis for the overall conversion of  $\text{CO}_2$  to acetate and ethanol (Fig. 1A). An adapted strain of *Cl* was developed and shows improved syngas-to-acetate conversion. The syngas for fermentation by *Cl* was subsequently sourced from a synthetic  $\text{CO}_2$ -to-syngas photocatalyst to demonstrate an overall  $\text{CO}_2 \rightarrow \text{syngas} \rightarrow \text{acetate}$  domino-reaction. We therefore present a novel approach for solar energy storage in multicarbon chemicals and biomass that harnesses the symbiotic strength of synthetic and biological catalysts.



## Experimental Section

### Materials and chemicals

Deuterium oxide ( $D_2O$ ) solution (99.9 atom% D) containing 0.05 wt. or 0.75 wt% 3-(trimethylsilyl)propionic-2,2,3,3- $d_4$  acid, sodium salt, triethanolamine (TEOA,  $\geq 99.0\%$ ) and glycerol (for molecular biology,  $\geq 99.0\%$ ) as well as all chemicals used for bacterial growth and the isotopically labelled gases  $^{13}CO_2$  and  $^{13}CO$  were purchased from Sigma-Aldrich.  $TiO_2$  powder P25 (10–30 nm diameter;  $50\text{ m}^2\text{ g}^{-1}$ ) was obtained from Evonik.  $[Co(2,2':6',2''\text{-terpyridine-4'-phosphonic acid})_2](BF_4)_2$  (denoted as **CotpyP**) was synthesized and characterized according to reported procedures.<sup>21</sup> Reaction gases  $CO_2$  with 2%  $CH_4$  as internal gas chromatography standard, and synthesis gas (syngas) cylinders (25%  $CO$ , 10%  $H_2$ , 65%  $CO_2$ ) were purchased from Brin's Oxygen Company (BOC).

### Bacteria growth, syngas adaptation, storage and handling

*Clostridium ljungdahlii* (*Cl*) DSMZ 13528 was purchased from The Leibniz Institute DSMZ (German Collection of Microorganisms and Cell Cultures GmbH). Cultures were initially grown in ATCC Medium 1754, which contained essential nutrients and vitamins, supplemented with  $5.00\text{ g L}^{-1}$  fructose as a carbon source to establish initial growth conditions conducive to syngas adaptation. The specific setups for feeding syngas (Fig. S1†), including batch and continuous flow modes, were designed to mimic industrial conditions and evaluate the strains' performance under varying operational parameters.

The adaptation to syngas was conducted in a two-stage process. In the first stage, freshly cultured wild-type *Cl* ( $Cl_{wt}$ ) cells were acclimatized to a syngas environment by gradually decreasing the fructose concentration in the ATCC Medium 1754 over nine consecutive transfers, each lasting 72 hours. This gradual reduction aimed to incrementally expose the microbial population to syngas with less dependency on the fructose, thereby selecting for cells with enhanced syngas utilization capabilities. The syngas (25%  $CO$ , 10%  $H_2$ , 65%  $CO_2$ ) roughly mimics the syngas ratios obtained in typical industrial processes, such as biomass gasification, and state-of-the-art electrolysis systems.<sup>22,23</sup> In the second stage, cultures were exclusively grown on syngas without any fructose supplementation for an additional 11 transfers. This stringent selection pressure ensured the enrichment of syngas-adapted phenotypes capable of sustained growth and metabolism solely on syngas.

Post-adaptation, the adapted *Cl* culture, designated as  $Cl_{adapt}$  (internal strain registration name as RLM034 for strain request), and the wild-type control,  $Cl_{wt}$  (internal strain registration name as RLM028 for strain request), were stored for long-term preservation. Cultures were mixed with an equal volume of sterile 40% glycerol solution (in  $ddH_2O$ ) to achieve a final concentration of 20% glycerol and stored at  $-80\text{ }^\circ\text{C}$ . This method ensured the viability and genetic stability of the microbial samples for future analyses and experiments.

During bacterial cultivation and transfers, the medium bottles were continuously purged with  $N_2$  to minimize  $O_2$  exposure. Additionally, when taking optical density (OD) and

nuclear magnetic resonance (NMR) samples, the medium bottles remained under syngas purging, further preventing oxygen intrusion.

### Optical density, product quantification, and isotopic labelling

The optical density was monitored at 600 nm ( $OD_{600}$ ) to assess cell growth and adaptation progress at each transfer stage using an ultraviolet-visible (UV-vis) spectrophotometer (Agilent Cary 60).

Gaseous  $H_2$  and  $CO$  in the headspace were analyzed by gas chromatography using a Shimadzu Tracer GC-2010 Plus with a barrier discharge ionization detector, equipped with a Shin-Carbon micro-ST Column (0.53 mm diameter) kept at  $40\text{ }^\circ\text{C}$  using Helium carrier gas. Typically, 20, 50 or 100  $\mu\text{L}$  of headspace gas were injected using a gas-tight syringe (Hamilton). The response factors for the gases were determined by calibration with known amounts of  $H_2$  and  $CO$ .

Fructose consumption and the production of formate, acetate and other  $C_2$  compounds, indicative of the metabolic activity and efficiency of syngas conversion by the adapted and wild-type strains, were quantified by quantitative  $^1H$  nuclear magnetic resonance (qNMR) spectroscopy using a Bruker 400 MHz Neo Prodigy Spectrometry. The chemical shift ( $\delta$ ) of the  $^1H$  NMR spectrum is referenced against the internal standard 3-(trimethylsilyl)propionic-2,2,3,3- $d_4$  acid, sodium salt (0.05 wt% or 0.75 wt% in  $D_2O$ ). To prepare a typical NMR solution, 570  $\mu\text{L}$  of a filtered aliquot (0.22  $\mu\text{m}$  syringe filter) from the bacteria culture was combined with 30  $\mu\text{L}$  of the internal standard solution in an NMR tube.

For isotopic labelling experiments, a sealed bottle containing a bacterial culture of  $Cl_{adapt}$  in ATCC Medium 1754 (modified) was purged with  $^{13}C$ -labelled syngas gas (65%  $^{13}CO_2$ /25%  $^{13}CO$ /10%  $H_2$ ) using mass flow controllers (Alicat Scientific). The ATCC Medium 1754 was modified by changing the  $NaH^{12}CO_3$  into  $NaH^{13}CO_3$ , for the purpose of  $^{13}C$  labelling. When indicated, 30 mM of  $^{13}C$ -formate was also added into the medium. The culture was kept in a shaker-incubator with a constant temperature of  $37\text{ }^\circ\text{C}$  and shaking (150 rpm) for 12 days. Subsequently, the products in the media were characterized by  $^1H$  NMR spectroscopy as described above.

### Calculation on growth rate and doubling time

The growth rate is highest and most consistent during the exponential phase. The growth rate ( $\mu$ ) can be calculated using the formula:

$$\mu = \frac{\Delta \ln(OD)}{\Delta t} = \frac{\ln(OD_{t_2}) - \ln(OD_{t_1})}{(t_2 - t_1)}$$

where  $\Delta \ln(OD)$  is the change in the natural logarithm of OD, and  $\Delta t$  is the change in time (difference between time point 1 ( $t_1$ ) and 2 ( $t_2$ )).

A python script was developed to analyze bacterial growth from optical density (OD) measurements over time. It automatically detects the exponential growth phase within a given time range, calculates the growth rate and doubling time, and



plots the growth curve with the exponential fit. Source code is available on <https://github.com/su2lin/microbiology>.

## Sequencing

Whole Genome Sequencing (WGS) of the adapted strain ( $Cl_{\text{adapt}}$ ) and its wild-type counterpart ( $Cl_{\text{wt}}$ ) was performed to identify genomic variations associated with enhanced syngas fermentation capabilities. Sequencing and analysis were conducted by GENEWIZ. For each strain, a single cell pellet sample was prepared by centrifuging 13 mL of liquid culture to remove the culture medium. The resulting pellets were resuspended in DNA/RNA Shield reagent (Zymo Research Corporation), flash-frozen in liquid nitrogen for stability, and shipped on dry ice to ensure sample integrity during transit.

For WGS data processing, raw sequencing reads were initially assessed for quality using FastQC. Poor quality reads and bases were then filtered and trimmed using Trimmomatic. The quality-filtered reads were mapped to the *C. ljungdahliae* reference genome using the Burrows Wheeler Aligner (BWA), which is designed for mapping low-divergent sequences against large reference genomes. The resulting SAM files were converted to BAM format and indexed using samtools to facilitate visualization of the alignments. Finally, single nucleotide variants (SNVs) were detected using bcftools. This comprehensive bioinformatics pipeline—encompassing quality control, trimming, mapping, indexing, and SNV detection—ensured accurate identification of genomic variations between  $Cl_{\text{adapt}}$  and  $Cl_{\text{wt}}$ .

## Photocatalytic syngas production

In a typical experiment, an aqueous suspension containing  $\text{TiO}_2$  (P25, 365 mg) and **CotpyP** ( $20 \mu\text{mol g}_{\text{TiO}_2}^{-1}$ ) in 0.22 L of 0.1 M TEOA solution ( $\text{pH} \approx 7$ ) was added to a scaled-up photoreactor<sup>24</sup> (total volume = 1.52 L, Fig. S2†). Then, the photocatalytic suspension was purged under stirring (400 rpm) with  $\text{CO}_2$ , containing 2%  $\text{CH}_4$  as gas chromatography internal standard, for 45 min. The stirred photoreactor was subsequently irradiated from the top with a solar light simulator (G2V Sunbrick LED Solar Simulator) with  $\lambda = 366 \text{ nm}$  to  $423 \text{ nm}$  ( $20.4 \text{ mW cm}^{-2}$ ) for 24 h at ambient temperature. The irradiation provided by the solar light simulator for  $\lambda = 366\text{--}423 \text{ nm}$  is consistent with AM1.5 G irradiation, but wavelengths  $\lambda > 423 \text{ nm}$  were removed to avoid unnecessary heating of the photoreactor.

The photocatalytic process was monitored by analyzing the headspace (volume = 1.30 L) after completion (24 h, batch mode experiment) or every 24 h (flow mode experiment) to monitor  $\text{H}_2$  and  $\text{CO}$  formation using a gas chromatograph (see above). For the batch mode experiments, after 24 h of irradiation, the photoreactor was connected for 6 days to a bioreactor containing  $\approx 13 \text{ mL}$  of ATCC Medium 1754 with the adapted bacterial strain. For the flow mode experiments, the photoreactor was connected before solar light irradiation to three bioreactors and during irradiation,  $\text{CO}_2$  was flowed using a mass flow controller (Alicat) at a constant flow rate  $30 \text{ mL min}^{-1}$  and every 24 h, a fresh batch of  $20 \mu\text{mol CotpyP}$

$\text{g}_{\text{TiO}_2}^{-1}$  was added into the photoreactor. Photocatalysis batch and flow experiments were performed in triplicates.

## Statistical analysis

The mean ( $\bar{x}$ ) with its standard deviation ( $\sigma_{\bar{x}}$ ) expressed as  $\bar{x} \pm \sigma_{\bar{x}}$  from  $n$  ( $n \geq 3$ ) independent experiments ( $x_i$ ). The standard errors were calculated using OriginPro 2024 (OriginLab).

$$\bar{x} = \frac{1}{n} \sum_{i=1}^n x_i$$

$$\sigma_{\bar{x}} = \sqrt{\frac{1}{(n-1)} \sum_{i=1}^n (x_i - \bar{x})^2}$$

# Results and discussion

## Microbial adaptation to syngas fermentation

The wild-type *C. ljungdahliae* was initially cultured in ATCC Medium 1754 with  $5.0 \text{ g L}^{-1}$  fructose and preserved with 20% glycerol at  $-80^\circ\text{C}$  ( $Cl_{\text{wt}}$ ). ALE was performed over 20 transfers (Fig. 1B): transfers 1–9 involved gradual fructose reduction under constant syngas (25%  $\text{CO}$ , 10%  $\text{H}_2$ , 65%  $\text{CO}_2$ , 112 mL headspace), followed by 11 transfers using syngas exclusively. Each 72 hour transfer was conducted at  $37^\circ\text{C}$  and 150 rpm, with  $\text{OD}_{600}$  monitored to confirm consistent growth (Fig. S3 and S4†). The final adapted culture was designated  $Cl_{\text{adapt}}$ .

To validate the success of ALE, we assessed bacterial growth on syngas under batch and continuous flow conditions (Fig. S1†), simulating potential future application designs.<sup>24</sup> Cell populations were monitored *via*  $\text{OD}_{600}$  readings, and  $\text{C}_2$  products (acetate and ethanol) were quantified using quantitative  $^1\text{H}$  NMR (qNMR) spectroscopy (Fig. 1C and D). The adapted strain,  $Cl_{\text{adapt}}$ , exhibited faster growth (Fig. S5†) and higher final  $\text{OD}_{600}$  values than the wild-type  $Cl_{\text{wt}}$  in both modes. In batch mode,  $Cl_{\text{adapt}}$  reached an  $\text{OD}_{600}$  increase ( $\Delta\text{OD}_{600}$ ) of  $0.043 \pm 0.002$  by day 4, approximately 2.5 times higher than the  $0.017 \pm 0.003 \Delta\text{OD}_{600}$  of  $Cl_{\text{wt}}$ . In continuous flow mode, by day 6,  $Cl_{\text{adapt}}$  and  $Cl_{\text{wt}}$  recorded  $\text{OD}_{600}$  values of  $1.02 \pm 0.34$  and  $0.09 \pm 0.12$ , respectively, indicating an 11-fold increase in the adapted strain. Growth rate analysis (Table S1†) showed that  $Cl_{\text{adapt}}$  had rates of  $0.38 \pm 0.02$  per day in batch mode and  $0.96 \pm 0.11$  per day in flow mode, compared to  $Cl_{\text{wt}}$ 's slower rates of  $0.26 \pm 0.01$  and  $0.23 \pm 0.22$  per day, respectively (Fig. S6†). The enhanced growth of  $Cl_{\text{adapt}}$  under flow mode suggests improved syngas utilization following ALE, likely due to increased  $\text{CO}$  tolerance, as previous studies have shown high  $\text{CO}$  concentrations can impede growth rates.<sup>25,26</sup>

In batch mode (Fig. 1C),  $Cl_{\text{adapt}}$  produced  $0.27 \pm 0.01 \text{ mM}$  acetate and  $0.06 \pm 0.01 \text{ mM}$  ethanol over seven days, amounting to  $0.05 \pm 0.02 \text{ mM C}_2$  compounds per day from syngas. In contrast,  $Cl_{\text{wt}}$  produced  $0.06 \pm 0.01 \text{ mM}$  acetate and  $0.05 \pm 0.01 \text{ mM}$  ethanol, equivalent to  $0.02 \pm 0.01 \text{ mM C}_2$  compounds per day, approximately three-fold less than  $Cl_{\text{adapt}}$ , consistent with the observed growth rate differences. Under continuous flow mode (Fig. 1D),  $Cl_{\text{adapt}}$  generated  $69.1 \pm 28.3 \text{ mM}$  acetate and  $7.7 \pm 5.2 \text{ mM}$  ethanol in six days, translating to  $12.8 \pm$



5.6 mM C<sub>2</sub> compounds per day. In contrast, *Cl*<sub>wt</sub> generated 0.54 ± 0.70 mM acetate and 0.09 ± 0.03 mM ethanol, or 0.11 ± 0.12 mM C<sub>2</sub> compounds per day, approximately 120-fold lower than *Cl*<sub>adapt</sub>. This large discrepancy between these two modes of culture suggests that continuous flow conditions, providing sustained syngas availability, greatly enhance the performance of *Cl*<sub>adapt</sub>. Notably, under batch mode, ethanol production between the two strains showed no significant differences. However, under flow mode, the *Cl*<sub>adapt</sub> strain produced 85 times more ethanol than *Cl*<sub>wt</sub>, which may be attributed to the higher availability of reducing substrates (*i.e.*, CO and H<sub>2</sub>) in continuous flow conditions, facilitating the conversion of acetate into ethanol. Additionally, negative ethanol values observed in the first five days of continuous flow mode (Fig. 1D) resulted from the initial presence of ethanol in the growth medium and its subsequent consumption by the bacteria over time. These findings confirm the successful adaptation of *Cl*<sub>adapt</sub> to syngas, demonstrating significantly higher C<sub>2</sub> compound production, especially under continuous flow operation.

### Metabolic insights into carbon flux

To confirm the source of carbon in the C<sub>2</sub> products (Fig. 1A), we performed isotopic labelling experiments using <sup>13</sup>C-syngas as the sole substrate for *Cl*<sub>adapt</sub> and *Cl*<sub>wt</sub> over 12 days. The isotopologues were analyzed by qNMR spectroscopy (Fig. 2A, S7

and Tables S2, S3† for acetate, and Fig. S8 and Table S4, S5† for ethanol). *Cl*<sub>adapt</sub> and *Cl*<sub>wt</sub> showed acetate (38.2 and 5.3 mM) containing mixtures of <sup>13</sup>C and <sup>12</sup>C, including <sup>13</sup>CH<sub>3</sub>-<sup>13</sup>COO<sup>-</sup>, <sup>13</sup>CH<sub>3</sub>-<sup>12</sup>COO<sup>-</sup>, <sup>12</sup>CH<sub>3</sub>-<sup>13</sup>COO<sup>-</sup>, and <sup>12</sup>CH<sub>3</sub>-<sup>12</sup>COO<sup>-</sup>. However, only *Cl*<sub>adapt</sub> produced ethanol (0.7 mM) containing mixtures of <sup>13</sup>CH<sub>3</sub>-<sup>13</sup>CH<sub>2</sub>OH and <sup>12</sup>CH<sub>3</sub>-<sup>13</sup>CH<sub>2</sub>OH. For further discussion, see ESI Note 1.† The <sup>13</sup>C/<sup>12</sup>C ratios were 86 : 14 for acetate and 95 : 5 for ethanol in *Cl*<sub>adapt</sub>, and 70 : 30 for acetate in *Cl*<sub>wt</sub>, indicating that most of the carbon in the products originates from <sup>13</sup>C-syngas, with a smaller portion of <sup>12</sup>C likely coming from the parental culture or cellular carbon reserves. This finding confirms that both *Cl*<sub>adapt</sub> and *Cl*<sub>wt</sub> can produce C<sub>2</sub> compounds by converting the carbon in syngas. The higher <sup>13</sup>C content and the presence of ethanol as a more reduced product in *Cl*<sub>adapt</sub> indicates better syngas uptake and conversion activity than *Cl*<sub>wt</sub>.<sup>27</sup>

Notably, both strains produced less <sup>13</sup>CH<sub>3</sub>-<sup>12</sup>COO<sup>-</sup> than <sup>12</sup>CH<sub>3</sub>-<sup>13</sup>COO<sup>-</sup> (Table S3†), a metabolic preference that extended to <sup>12</sup>CH<sub>3</sub>-<sup>13</sup>CH<sub>2</sub>OH (Table S5†). This suggests a preference for retaining the <sup>12</sup>C-methyl rather than <sup>12</sup>C-carboxyl group. Compared to *Cl*<sub>wt</sub> (<sup>13</sup>CH<sub>3</sub>-<sup>12</sup>COO<sup>-</sup>/<sup>12</sup>CH<sub>3</sub>-<sup>13</sup>COO<sup>-</sup> = 0.9), the *Cl*<sub>adapt</sub> (<sup>13</sup>CH<sub>3</sub>-<sup>12</sup>COO<sup>-</sup>/<sup>12</sup>CH<sub>3</sub>-<sup>13</sup>COO<sup>-</sup> = 0.5) shows a more unbalanced <sup>12</sup>C/<sup>13</sup>C distribution. This observation may reflect a bottleneck in the *Cl*'s Wood-Ljungdahl pathway's methyl branch,<sup>28</sup> which *Cl*<sub>adapt</sub> has not yet overcome, or

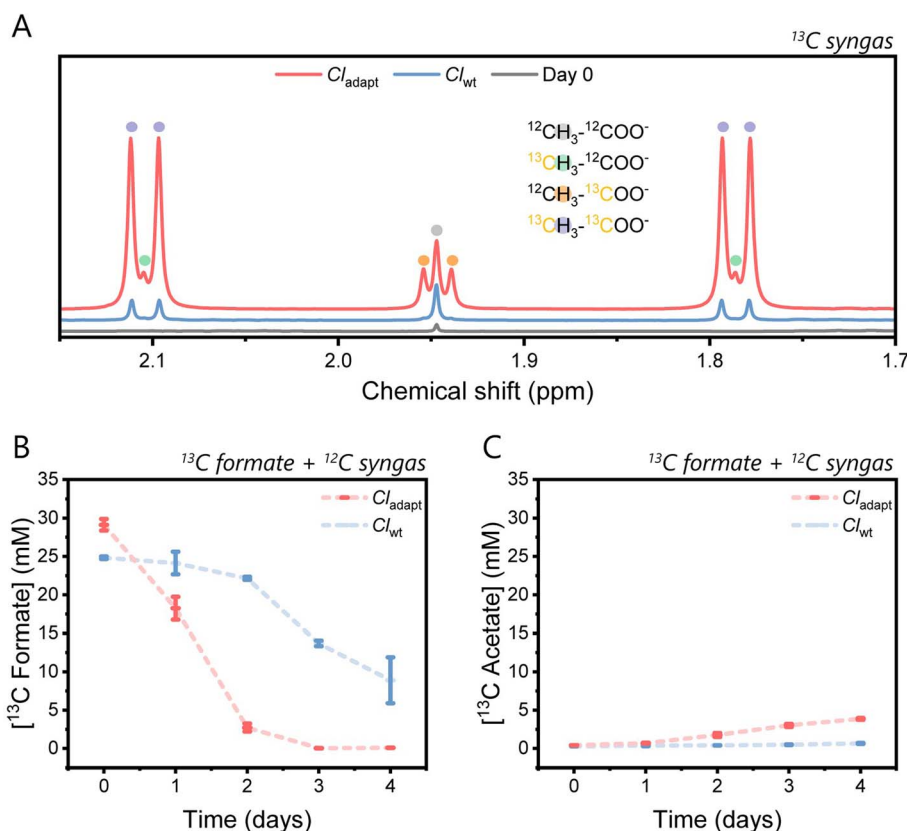


**Fig. 2** Growth analysis of strains using <sup>13</sup>C- and <sup>13</sup>C/<sup>12</sup>C mixed-substrates. (A) <sup>1</sup>H qNMR spectra showing acetate production by *Cl*<sub>adapt</sub> and *Cl*<sub>wt</sub>, when cultivated on <sup>13</sup>C-syngas (112 mL headspace) over 12 days. The isotopologues are color-coded based on the position of the <sup>13</sup>C atoms, as methyl or carboxyl, in acetate. (B) Consumption of <sup>13</sup>C-formate, and (C) production of <sup>13</sup>C-acetate, when cultivated on <sup>13</sup>C-formate (~30 mM) alongside <sup>12</sup>C-syngas (112 mL headspace) over 4 days. Growth conditions: ATCC Medium 1754 (pH 5.9), 37 °C with 150 rpm mixing.



alternatively the carbonyl branch has been significantly enhanced during adaptation.

To investigate differences in the methyl branch of the Wood–Ljungdahl pathway between  $Cl_{\text{adapt}}$  and  $Cl_{\text{wt}}$ , we performed a second isotopic labeling experiment using  $^{13}\text{C}$ -formate and  $^{12}\text{C}$ -syngas.  $Cl_{\text{adapt}}$  exhibited significantly faster growth, achieving a cell population five times greater than  $Cl_{\text{wt}}$  within four days (Fig. S9A†).  $Cl_{\text{adapt}}$  consumed  $\sim 25$  mM of  $^{13}\text{C}$ -formate within two days, whereas  $Cl_{\text{wt}}$  utilized only  $\sim 15$  mM over four days (Fig. 2B), resulting in a markedly higher production of  $^{13}\text{C}$ -acetate in  $Cl_{\text{adapt}}$  ( $3.86 \pm 0.11$  mM vs.  $0.66 \pm 0.06$  mM) (Fig. 2C). This finding highlights  $Cl_{\text{adapt}}$ 's enhanced efficiency in utilizing formate for such as growth and acetate production, reflecting optimized pathway dynamics compared to  $Cl_{\text{wt}}$ . For further discussion, see ESI Note 2 (Fig. S9 and 10).†

### Whole genome sequencing

We conducted whole genome sequencing analysis to investigate the genetic changes in  $Cl_{\text{adapt}}$  compared to  $Cl_{\text{wt}}$ . Whole genome sequencing of  $Cl_{\text{adapt}}$  and  $Cl_{\text{wt}}$  revealed several mutations compared to the reference genome in the NCBI database (Table S6, S7 and Fig. S11†). Notably, some mutations were present in both strains, suggesting that the wild-type strain had already diverged from the reference genome prior to our study. Additionally, mutations identified exclusively in  $Cl_{\text{adapt}}$  may have emerged either through the ALE process or as random variations in the single colony selected for sequencing. Similarly, the presence of unique mutations in  $Cl_{\text{wt}}$  suggests possible genetic drift or reversion events. Given these observations, future studies should validate key mutations through Sanger sequencing of multiple colonies to distinguish true evolutionary changes from colony-specific variations.

Notwithstanding these limitations—including the restricted sample numbers and incomplete functional annotation of some *C. ljungdahlii* genes—the molecular differences observed between  $Cl_{\text{adapt}}$  and  $Cl_{\text{wt}}$  suggest that the strains are distinct at a genetic level. While these differences may partly explain the variations observed in growth and  $\text{C}_2$  production, further studies are needed to establish a definitive link. For an in-depth analysis of the mutations differentiating  $Cl_{\text{adapt}}$  from  $Cl_{\text{wt}}$ , please refer to ESI Note 3.

### Photocatalytic domino valorization

To source syngas for microbial fermentation directly from solar  $\text{CO}_2$  conversion, we scaled up a previously reported photocatalytic system composed of light-absorbing  $\text{TiO}_2$  nanoparticles (P25) and a phosphonated cobalt(II)(terpyridine) $_2$   $\text{CO}_2$  reduction molecular catalyst (**CotpyP**,  $20 \mu\text{mol g}_{\text{TiO}_2}^{-1}$ ; Fig. 3).<sup>21,29</sup> The choice of this photocatalytic semiconductor-molecule hybrid system was based on its suitability for scale-up to produce sufficient syngas quantities and coupling with aqueous microbial fermentation: it consists of Earth-abundant elements and readily available light absorber ( $\text{TiO}_2$ ) and co-catalyst (**CotpyP**) components in the required quantities. The photocatalyst system is also robust and can be easily repaired by addition of fresh **CotpyP** (see Experimental Section). It is

therefore versatile and well suited for longer-term and multi-cycle experiments for aqueous  $\text{CO}_2$  photoreduction under batch<sup>30</sup> and flow conditions to couple with biocatalysis (see below; Table S8†).

We readily scaled-up this hybrid  $\text{TiO}_2$ |**CotpyP** photocatalyst from 5 mg to 365 mg without a significant effect in its catalytic activity during photocatalysis in the presence of triethanolamine (TEOA, 0.1 M) as sacrificial electron donor in water (0.22 L) using filtered simulated solar irradiation (see Experimental Section). The photoreactor used for scaling-up is cylindrical, with a surface area of  $217 \text{ cm}^2$  and a volume of 1.5 L (Fig. S2†). This photoreactor features a transparent top window that allows the simulated sunlight to photoexcite the semiconductor  $\text{TiO}_2$  nanoparticles, leading to electron transfer from  $\text{TiO}_2$  to the catalyst **CotpyP**. The reduced **CotpyP** reacts with aqueous  $\text{CO}_2$  resulting in the formation and release of  $\text{CO}$  and  $\text{H}_2$  gaseous products. Further details on the catalytic  $\text{CO}_2$  reduction

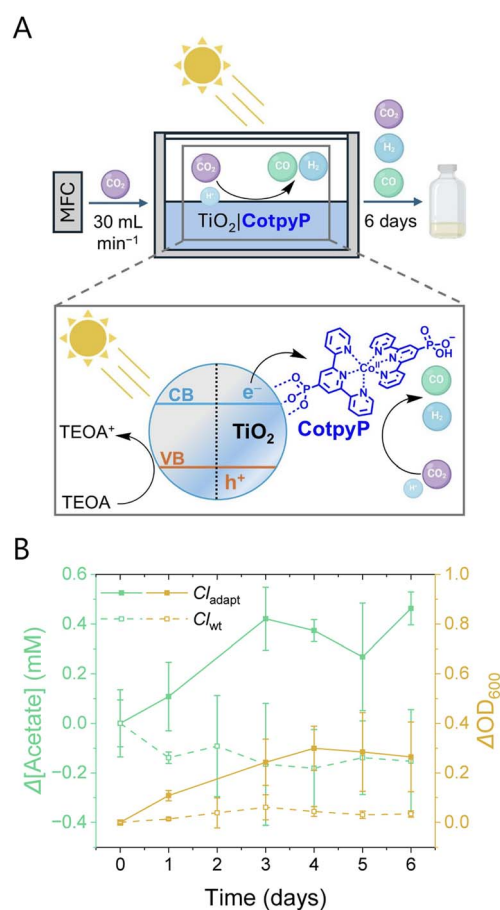


Fig. 3 Light-driven  $\text{CO}_2$  domino valorization system. (A) Scheme of flow mode setup: the mass flow controller (MFC) purges  $\text{CO}_2$  through the photoreactor, where  $\text{TiO}_2$ |**CotpyP** generates photocatalytically syngas in  $\text{CO}_2$ -saturated water containing TEOA (0.1 M). The photoreactor is irradiated by filtered simulated sunlight from the top; and the syngas output flows then through the bioreactor where bacteria are cultured. (B) Production of acetate and biomass by  $Cl_{\text{adapt}}$  (solid line) and  $Cl_{\text{wt}}$  (dotted line) in the bioreactor when connected to the photocatalytically produced syngas over 6 days, expressed as variation of acetate concentration and optical density ( $\text{OD}_{600}$ ).





mechanism of TiO<sub>2</sub>-bound **CotpyP** can be found in a previous report.<sup>21</sup> The positive charges (holes) formed in TiO<sub>2</sub> are neutralized through the oxidation of the sacrificial electron donor TEOA present in the solution, which regenerates the original ground state of the semiconductor and allows the photocatalytic cycle to repeat.

Finally, we coupled the scaled-up synthetic photocatalytic CO<sub>2</sub> reduction system to the syngas-fermenting *Cl<sub>adapt</sub>*, creating an inorganic-bacterial system capable of domino valorization of CO<sub>2</sub> into acetate and biomass with solar energy (Fig. 3A). The aqueous TiO<sub>2</sub>|**CotpyP** photocatalyst suspension (0.22 mL) was exposed to a flow of CO<sub>2</sub> over six days (flow mode), mimicking the flow conditions described above for fermentation, and the photogenerated syngas was continuously flowed from the photoreactor to the bioreactor (Fig. 3A; see also ESI Note 4 for batch mode experiment details).

In flow mode, TiO<sub>2</sub>|**CotpyP** produced syngas under irradiation and exhibited activities of  $148 \pm 97$  nmol CO g<sub>TiO<sub>2</sub></sub><sup>-1</sup> min<sup>-1</sup> and  $367 \pm 606$  nmol H<sub>2</sub> g<sub>TiO<sub>2</sub></sub><sup>-1</sup> min<sup>-1</sup> (Table S9†). The generated solar syngas had thus a CO : H<sub>2</sub> ratio of ~30 : 70 and TiO<sub>2</sub>|**CotpyP** under flow conditions produced 1.3 mmol of CO after 6 days of continuous experiment. Under dark conditions, TiO<sub>2</sub>|**CotpyP** was unable to produce syngas. Compared to other state-of-the-art photocatalytic flow systems, such as ZnSe-BF<sub>4</sub>|cobalt porphyrin, which produces  $19 \times 10^{-3}$  mmol of CO after 17 h,<sup>30</sup> and Bi<sub>2</sub>WO<sub>6</sub>, which produces  $1.2 \times 10^{-2}$  mmol of CO after 4 h,<sup>31</sup> TiO<sub>2</sub>|**CotpyP** exhibits a very high yield (Table S8†).

Syngas produced by TiO<sub>2</sub>|**CotpyP** allowed the *Cl<sub>adapt</sub>* cultures to increase their biomass from the start of the flow experiment until day 4, reaching a  $\Delta\text{OD}_{600}$  of  $0.30 \pm 0.09$ , which remained approximately constant until day 6 (Fig. 3B). In contrast to the batch mode (Fig. S12†), the flow configuration showed a rise in acetate from day 0 to day 6, with a maximum  $\Delta[\text{acetate}]$  of  $0.46 \pm 0.07$  mM (Fig. 3B). Under identical experimental conditions, *Cl<sub>wt</sub>* exhibited significantly lower performance, with a  $\Delta\text{OD}_{600}$  of only  $0.03 \pm 0.01$  and no acetate production after 6 days. The lack of ethanol production, lower  $\Delta\text{OD}_{600}$ , and  $\Delta[\text{acetate}]$  for *Cl<sub>adapt</sub>* can be attributed to the low syngas concentration (<0.1%) in the photocatalysis gas stream, as well as the slower formation rate by TiO<sub>2</sub>|**CotpyP** compared to direct feeding with a premixed syngas cylinder. As shown in Fig. 1D, *Cl<sub>adapt</sub>* achieves high biomass and C<sub>2</sub> product outputs under 10 mL of syngas per minute (which equals to 102  $\mu\text{mol CO min}^{-1}$  and 41  $\mu\text{mol H}_2 \text{ min}^{-1}$ ), highlighting the limitations of the presented photocatalytic configuration and the need for improved systems capable of delivering higher syngas formation rates to support *Cl<sub>adapt</sub>*.

Our results demonstrate that simple photocatalytic powder systems can be readily scaled up and, in principle, be used to supply solar syngas directly to gas-fermenting adapted bacteria. This approach offers an alternative to wired devices such as electrolyzers and photoelectrochemical cells.<sup>3,5,6,11</sup> Furthermore, these findings highlight the need for innovative renewable energy-driven syngas production systems and device architectures—such as advanced electrolyzers and photoelectrochemical systems—for researchers in biohybrids and domino catalysis. Future systems should be designed to bridge

the potential mismatch between syngas production and fermentation rates, maximizing the capabilities of gas-fermenting adapted bacteria to sustain high levels of C<sub>2</sub> production and cell growth over extended periods.

## Conclusions

The reported proof-of-concept semi-biological system demonstrates the integration of photocatalytic CO<sub>2</sub> reduction with adapted bacterial biosynthesis. Unlike previous nanomaterial-bacteria biohybrid systems that relied on ill-defined charge transfer pathways or photogenerated H<sub>2</sub>, our approach employs direct ALE-derived adaptation to achieve high C<sub>2</sub> product yields solely from syngas produced from solar CO<sub>2</sub> reduction. This work illustrates the scalability of photocatalytic powder systems and underscores the simplicity of implementing adaptive evolution in a chemistry laboratory, thereby enhancing the microorganisms' natural capabilities while seamlessly coupling them with inorganic catalytic systems. While our sequencing analysis of the ALE-derived strain has limitations—stemming from restricted sample numbers and incomplete functional annotation—it provides initial insights into the genomic changes that may underpin the observed phenotypic improvements. Future investigations will be essential to pinpoint the key genes responsible for faster growth and higher product yields, as well as to optimize these biological-inorganic hybrid systems by improving syngas formation rates, eliminating the sacrificial electron donor in the photocatalysis process, and advancing genetic and metabolic engineering strategies. Overall, this study highlights the transformative potential of combining innovations from biology, materials science, and chemistry to address critical global environmental challenges.

## Data availability

Experimental data supporting the findings of this study are available from the University of Cambridge data repository (<https://doi.org/10.17863/CAM.118249>).

## Author contributions

Lin Su conceptualization, data curation, formal analysis, funding acquisition, investigation, visualization, methodology, project administration, writing – original draft, review & editing; Santiago Rodríguez-Jiménez conceptualization, data curation, formal analysis, funding acquisition, investigation, visualization, methodology, project administration, writing – original draft, review & editing; Marion I. M. Short investigation, methodology, writing – review & editing; Erwin Reisner conceptualization, resources, formal analysis, supervision, funding acquisition, validation, investigation, visualization, project administration, writing – original draft, review & editing.

## Conflicts of interest

There are no conflicts to declare.





## Acknowledgements

This work was supported by UK Research & Innovation (UKRI, ERC Advanced Grant, EP/X030563/1 to E. R.), the UK Department of Science, Innovation & Technology and the Royal Academy of Engineering Chair in Emerging Technologies programme (CIET-2324-83 to E. R.), a Leverhulme Trust Early Career Fellowship (ECF-2022-392 to L. S.), the Isaac Newton Trust (22.08(c) to L. S.), a European Commission Marie Skłodowska-Curie Individual Fellowship (GAN 891338 to S. R. J.), and the Engineering and Physical Sciences Research Council (EPSRC) for a NanoDTC PhD scholarship (EP/L015978/1 to M. I. M. S.). The authors thank Mr Dongseok Kim and Dr Leonardo Castañeda-Losada at the University of Cambridge for helpful discussion.

## References

- 1 X. Fang, S. Kalathil and E. Reisner, *Chem. Soc. Rev.*, 2020, **49**, 4926–4952.
- 2 N. Kornienko, J. Z. Zhang, K. K. Sakimoto, P. Yang and E. Reisner, *Nat. Nanotechnol.*, 2018, **13**, 890–899.
- 3 C. Liu, B. C. Colón, M. Ziesack, P. A. Silver and D. G. Nocera, *Science*, 2016, **352**, 1210–1213.
- 4 S. F. Rowe, G. L. Gall, E. V. Ainsworth, J. A. Davies, C. W. J. Lockwood, L. Shi, A. Elliston, I. N. Roberts, K. W. Waldron, D. J. Richardson, T. A. Clarke, L. J. C. Jeuken, E. Reisner and J. N. Butt, *ACS Catal.*, 2017, **7**, 7558–7566.
- 5 H. Zhang, H. Liu, Z. Tian, D. Lu, Y. Yu, S. Cestellos-Blanco, K. K. Sakimoto and P. Yang, *Nat. Nanotechnol.*, 2018, **13**, 900–905.
- 6 K. K. Sakimoto, A. B. Wong and P. Yang, *Science*, 2016, **351**, 74–77.
- 7 M. Köpke, C. Held, S. Hujer, H. Liesegang, A. Wiezer, A. Wollherr, A. Ehrenreich, W. Liebl, G. Gottschalk and P. Dürre, *Proc. Natl. Acad. Sci. U. S. A.*, 2010, **107**, 13087–13092.
- 8 L. Zhang, R. Zhao, D. Jia, W. Jiang and Y. Gu, *Curr. Opin. Chem. Biol.*, 2020, **59**, 54–61.
- 9 S. Schulz, B. Molitor and L. T. Angenent, *Bioresour. Technol.*, 2023, **369**, 128387.
- 10 F. E. Liew, R. Nogle, T. Abdalla, B. J. Rasor, C. Canter, R. O. Jensen, L. Wang, J. Strutz, P. Chirania, S. D. Tissera, A. P. Mueller, Z. Ruan, A. Gao, L. Tran, N. L. Engle, J. C. Bromley, J. Daniell, R. Conrado, T. J. Tschaplinski, R. J. Giannone, R. L. Hettich, A. S. Karim, S. D. Simpson, S. D. Brown, C. Leang, M. C. Jewett and M. Köpke, *Nat. Biotechnol.*, 2022, **40**, 335–344.
- 11 T. Haas, R. Krause, R. Weber, M. Demler and G. Schmid, *Nat. Catal.*, 2018, **1**, 32–39.
- 12 V. A. Portnoy, D. Bezdan and K. Zengler, *Curr. Opin. Biotechnol.*, 2011, **22**, 590–594.
- 13 M. Dragosits and D. Mattanovich, *Microb. Cell Factories*, 2013, **12**, 64.
- 14 T. M. Wannier, A. M. Kunjapur, D. P. Rice, M. J. McDonald, M. M. Desai and G. M. Church, *Proc. Natl. Acad. Sci. U. S. A.*, 2018, **115**, 3090–3095.
- 15 S. Kang, Y. Song, S. Jin, J. Shin, J. Bae, D. R. Kim, J.-K. Lee, S. C. Kim, S. Cho and B.-K. Cho, *Front. Microbiol.*, 2020, **11**, 402.
- 16 J. Kim, S. Cestellos-Blanco, Y. Shen, R. Cai and P. Yang, *Nano Lett.*, 2022, **22**, 5503–5509.
- 17 K. Wang, Y. Liu, Z. Wu, Y. Wu, H. Bi, Y. Liu, M. Wang, B. Chen, J. Nielsen, Z. Liu and T. Tan, *Green Carbon*, 2023, **1**, 65–74.
- 18 T. Lechtenberg, B. Wynands, M.-F. Müller, T. Polen, S. Noack and N. Wierckx, *Metab. Eng. Commun.*, 2024, **18**, e00235.
- 19 H. Ingelman, J. K. Heffernan, A. Harris, S. D. Brown, K. M. Shaikh, A. Y. Saqib, M. J. Pinheiro, L. A. de Lima, K. R. Martinez, R. A. Gonzalez-Garcia, G. Hawkins, J. Daleiden, L. Tran, H. Zeleznik, R. O. Jensen, V. Reynoso, H. Schindel, J. Janes, S. D. Simpson, M. Kopke, E. Marcellin and K. Valgepea, *New Biotechnol.*, 2024, **83**, 1–15.
- 20 J. Heffernan, R. A. G. Gonzalez, V. Mahamkali, T. McCubbin, D. Daygon, L. Liu, R. Palfreyman, A. Harris, M. Koepke, K. Valgepea, L. K. Nielsen and E. Marcellin, *Microb. Biotechnol.*, 2024, **17**, e14452.
- 21 J. J. Leung, J. Warnan, K. H. Ly, N. Heidary, D. H. Nam, M. F. Kuehnelt and E. Reisner, *Nat. Catal.*, 2019, **2**, 354–365.
- 22 S. Lamaison, D. Wakerley, F. Kracke, T. Moore, L. Zhou, D. U. Lee, L. Wang, M. A. Hubert, J. E. A. Acosta, J. M. Gregoire, E. B. Duoss, S. Baker, V. A. Beck, A. M. Spormann, M. Fontecave, C. Hahn and T. F. Jaramillo, *Adv. Mater.*, 2022, **34**, e2103963.
- 23 R. Takors, M. Kopf, J. Mampel, W. Bluemke, B. Blombach, B. Eikmanns, F. R. Bengelsdorf, D. Weuster-Botz and P. Dürre, *Microb. Biotechnol.*, 2018, **11**, 606–625.
- 24 S. Linley and E. Reisner, *Adv. Sci.*, 2023, **10**, 2207314.
- 25 B. H. Kim, P. Bellows, R. Datta and J. G. Zeikus, *Appl. Environ. Microbiol.*, 1984, **48**, 764–770.
- 26 M. T. Allaart, M. Diender, D. Z. Sousa and R. Kleerebezem, *Microb. Biotechnol.*, 2023, **16**, 697–705.
- 27 M. Diender, A. J. M. Stams and D. Z. Sousa, *Biotechnol. Biofuels*, 2016, **9**, 82.
- 28 N. Fackler, B. D. Heijstra, B. J. Rasor, H. Brown, J. Martin, Z. Ni, K. M. Shebek, R. R. Rosin, S. D. Simpson, K. E. Tyo, R. J. Giannone, R. L. Hettich, T. J. Tschaplinski, C. Leang, S. D. Brown, M. C. Jewett and M. Köpke, *Annu. Rev. Chem. Biomol. Eng.*, 2021, **12**, 1–32.
- 29 E. Lam and E. Reisner, *Angew. Chem., Int. Ed.*, 2021, **60**, 23306–23312.
- 30 C. D. Sahm, G. M. Ucoski, S. Roy and E. Reisner, *ACS Catal.*, 2021, **11**, 11266–11277.
- 31 C. S. Ribeiro, J. Z. Y. Tan, M. M. Maroto-Valer and M. A. Lansarin, *J. Environ. Chem. Eng.*, 2021, **9**, 105097.

